Geometric dephasing in zero-field magnetic resonance

J. A. Jones[a)]
Oxford Centre for Molecular Sciences, University of Oxford, New Chemistry Laboratory, South Parks Road, Oxford OX1 3QT, and Merton College, Oxford OX1 4JD, United Kingdom

A. Pines
Lawrence Berkeley Laboratory and Department of Chemistry, University of California, Berkeley, California 94720

(Received 16 September 1996; accepted 19 November 1996)

Geometric phases acquired randomly can give rise to coherence dephasing in nuclear spin systems, equivalent to spin relaxation. We calculate the form and extent of this geometric dephasing in a number of model systems involving the motion of ^{131}Xe nuclei in shaped containers. The dephasing is calculated in two ways: first, using an analytical treatment of the diffusive motion of individual nuclei, and second, using ensemble averaged propagators. The effects of applying additional magnetic fields to these systems are discussed briefly. © *1997 American Institute of Physics.* [S0021-9606(97)01408-6]

I. INTRODUCTION

In conventional high-field magnetic resonance the nuclear spin Hamiltonian is dominated by the large Zeeman term, and other terms (such as dipole–dipole couplings or quadrupolar interactions) act as small perturbations. The total Hamiltonian depends on the relative orientation of the magnetic field and the perturbing Hamiltonian (generally referred to some molecular coordinate system), and so the nuclear spin energy levels, and hence the transition frequencies, depend on molecular orientation. Interactions of this kind are said to be *anisotropic*, and in randomly oriented samples, such as powders, they give rise to broad spectral lines.

In mobile phases molecular motion affects the relative orientation of the field and the perturbing molecular spin Hamiltonian, thus modulating the nuclear spin energy levels. If the motion is fast compared with the width of the distribution of energy levels, the Hamiltonian will be averaged, resulting in narrower lines; if the motion is isotropic (for example, molecular tumbling in liquids) the Hamiltonian will be completely averaged to its isotropic value. The underlying anisotropy does, however, remain important, as it is a major source of relaxation: Components of the Hamiltonian which are modulated at the frequency of a nuclear spin transition give rise to transitions, resulting in relaxation.

In zero-field magnetic resonance the absence of an external field automatically renders the interactions isotropic. The choice of any external or molecular coordinate system is arbitrary, and so the nuclear spin energy levels cannot depend on orientation. It might therefore seem that adiabatic motion of the system cannot have any effect on the resonance; however, as shown by Berry,[1–3] such an assumption is not correct. While adiabatic motions do not change the energy levels (the eigenvalues of the Hamiltonian), they affect the states (the eigenvectors), thereby giving rise to phase shifts and to transitions between quantum states.

The phase shifts can be detected directly using interference experiments,[4,5] but an alternative approach, useful in magnetic resonance, is to consider their effect on transition moments. If motion causes two spin states to acquire different phase shifts, then the coherent superposition of these states will acquire a phase shift equal to the difference between the two individual shifts. If the motion is continuous and coherent, then the transition phase shift will increase linearly with time, which is equivalent to a change in the transition frequency. In this manner, Berry's phase gives rise to frequency shifts and splittings.[6,7] If the motion is incoherent, the resulting random acquisition of Berry's phase could give rise to coherence dephasing, which is equivalent to spin relaxation.[8] Here, we calculate the extent of this relaxation in pure nuclear quadrupole resonance (NQR) studies of ^{131}Xe gas.

II. THEORY

In Berry's original paper,[1] and in many subsequent treatments,[2] Berry's phase was treated as a necessary *geometric* phase correction to the *dynamic* phase calculated using the adiabatic approximation.[9] In zero-field magnetic resonance, motion will not change the essential form of the Hamiltonian, or its magnitude, but will only change the orientation of its principal axes. Berry solved this problem by calculating the evolution under a static Hamiltonian and then adding a correction term arising from the motion. It is also possible to transform the problem into a frame of reference whose motion exactly matches the motion of the Hamiltonian, so that in this new frame the Hamiltonian is indeed static. As this transformation is a gauge transformation, it will modify the Hamiltonian by the addition of a gauge field. The Hamiltonian, $\mathscr{H}$, must be replaced by

$$\mathscr{H}^R = U^{-1}\mathscr{H}U - iU^{-1}\dot{U}, \tag{1}$$

[a)]To whom correspondence should be addressed at the New Chemistry Laboratory. Electronic mail: jones@bioch.ox.ac.uk

where U is a unitary matrix describing the transformation into the moving frame and $\hbar$ has been set equal to unity. The first term has the same form as the original Hamiltonian (now static), while the second term is the additional gauge field. For continuous rotation around some axis, α, the appropriate transformation is $U=\exp(-i\omega_R I_\alpha t)$, where ω_R is the rotation rate, and so the gauge field, $-\omega_R I_\alpha$, has the form of a ''fictitious magnetic field'' along the rotation axis (this behavior is familiar in high-field magnetic resonance, where transformation into a rotating frame acts to reduce or remove the Zeeman field).

Clearly the effect of this fictitious magnetic field will depend on the form of the static Hamiltonian, which for gaseous ^{131}Xe in zero field is the quadrupolar interaction, a system studied extensively in Princeton.[10] The ^{131}Xe nucleus has spin $I=\frac{3}{2}$, and its energy levels are split into two degenerate pairs in the presence of an electric field gradient. Most nuclei in a gas sample do not experience a field gradient, but those near the walls of the container experience a substantial field gradient, and in small containers rapid exchange of gas atoms between wall sites and the interior causes the nuclei to experience a net quadrupolar coupling to the entire container.[10,11] Clearly the details of this coupling will depend on the size and shape of the container. For a cylindrical container the coupling will be axially symmetric, with the symmetry axis lying along the axis of the cylinder. The magnitude of the coupling is largest for cylinders in which at least one of the spatial dimensions is sufficiently small that the gas atoms are close to a container wall much of the time.

This situation has been extensively studied in Princeton and Stuttgart. In the Stuttgart experiments,[7,12,13] designed to implement an NMR gyroscope, the container is a flat cylinder of approximately 20 mm diameter and 2 mm height, giving rise to a quadrupole splitting of about 0.5 Hz. Clearly, such small splittings cannot be detected by conventional means, but optical pumping and detection[10,11] allow the splitting to be readily measured. The details can be found elsewhere,[7,12,13] but the principles can be easily summarized. Optical pumping in the presence of a static field is used to create a substantial spin magnetization along some axis. This magnetization is then allowed to evolve freely under the quadrupolar Hamiltonian, and the magnetization remaining is detected optically. This time-domain signal is then Fourier transformed to obtain the NQR signal.

For a static container the quadrupolar Hamiltonian is most conveniently written in an axis system whose z axis is aligned with the symmetry axis of the quadrupolar interaction

$$\mathscr{H}=\omega_Q[I_z^2-\tfrac{1}{3}I(I+1)], \tag{2}$$

where ω_Q is the size of the average quadrupolar coupling. This has eigenvalues of $\pm\omega_Q$, and allowed transitions with frequencies of 0 and $2\omega_Q$. Appelt *et al.* have studied the effect of rotating the container about some axis while observing the NQR spectrum,[12] a system closely related to that of Tycko.[6] Suppose the container is rotated around an axis at right angles to the container axis. This axis may be arbitrarily assigned as the x axis, and the Hamiltonian in the rotating frame must then be modified by the addition of a gauge field, $-\omega_R I_x$, where ω_R is the rotation rate. Hence

$$\mathscr{H}^R=\omega_Q[I_z^2-\tfrac{1}{3}I(I+1)]-\omega_R I_x. \tag{3}$$

This can be expanded in the normal basis set to give

$$\mathscr{H}^R=\begin{pmatrix} \omega_Q & \frac{-\sqrt{3}}{2}\omega_R & 0 & 0 \\ \frac{-\sqrt{3}}{2}\omega_R & -\omega_Q & -\omega_R & 0 \\ 0 & -\omega_R & -\omega_Q & \frac{-\sqrt{3}}{2}\omega_R \\ 0 & 0 & \frac{-\sqrt{3}}{2}\omega_R & \omega_Q \end{pmatrix}. \tag{4}$$

While this matrix can be diagonalized directly,[12] a much simpler result can be achieved by assuming that the motion is adiabatic (see Fig. 1). If $|\omega_R|\ll|\omega_Q|$, then four of the off diagonal elements in Eq. (4) can be ignored, giving the much simpler adiabatic Hamiltonian

$$\mathscr{H}^R_{\mathrm{ad}}=\begin{pmatrix} \omega_Q & 0 & 0 & 0 \\ 0 & -\omega_Q & -\omega_R & 0 \\ 0 & -\omega_R & -\omega_Q & 0 \\ 0 & 0 & 0 & \omega_Q \end{pmatrix}. \tag{5}$$

This has eigenvalues of ω_Q, ω_Q, and $-\omega_Q\pm\omega_R$, and so the allowed transition at frequency $2\omega_Q$ will be split into two, with frequencies $2\omega_Q\pm\omega_R$, that is, a splitting of $2\omega_R$.

Within the adiabatic limit the fictitious field only affects the $|\pm\frac{1}{2}\rangle$ levels, and so it is appropriate to treat these central levels as a fictitious spin-$\frac{1}{2}$. Note, however, that a true spin-$\frac{1}{2}$ nucleus would be split by the field to give eigenstates separated by $\pm\frac{1}{2}\omega_R$, only half the splitting observed in this case.

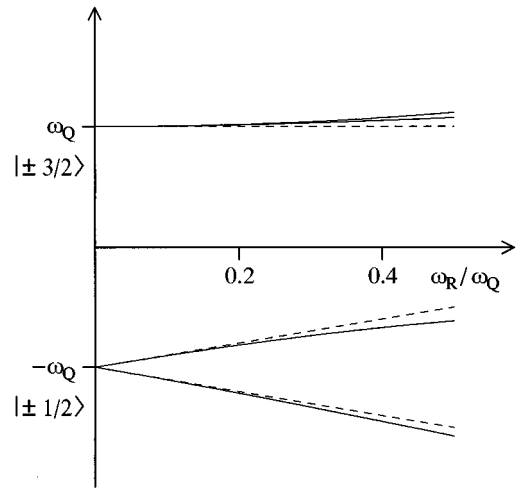

FIG. 1. Application of a magnetic field perpendicular to an axially symmetric quadrupolar interaction in a spin-$\frac{3}{2}$ nucleus. The solid lines show the exact result obtained by diagonalizing Eq. (4), while the dashed lines were calculated by diagonalizing the approximate adiabatic Hamiltonian shown in Eq. (5). If $|\omega_R|\ll|\omega_Q|$ the major effect is to split the $|\pm\frac{1}{2}\rangle$ levels, with a splitting $2\omega_R$, while the $|\pm\frac{3}{2}\rangle$ levels remain largely unaffected.

This effect is equivalent to a well known effect in high-field NMR studies of quadrupolar nuclei:[14–16] When a half-odd-integer spin nucleus is excited with a weak radio frequency field, which only excites the central transition, the effective field strength is increased by a factor of $I+\frac{1}{2}$.

The exact form of the signal observed in an optically detected experiment obviously depends on the choice of initial state and detection operator. Throughout this paper we make a particularly simple choice: We choose both the initial state and the detected state to consist of Zeeman magnetization along the rotation axis. This has the major computational advantage that the detection operator is not affected by the rotating frame transformation, and also corresponds to a sensible choice in a possible experiment we discuss below. Other choices of initial state and detection operator will, of course, give slightly different results, but the broad principles described below will still apply. With this choice of initial state and detection operator, we may calculate the NQR signal observed from a rotating cylinder as

$$s(t)=\mathrm{tr}[I_x e^{-i\mathscr{H}^R_{\mathrm{ad}}t} I_x e^{i\mathscr{H}^R_{\mathrm{ad}}t}] \tag{6}$$

$$=2+3\cos(2\omega_Q t)\cos(\omega_R t). \tag{7}$$

This situation can be generalized to consider rotation around an axis at some arbitrary angle θ to the quadrupolar axis. In this case the Hamiltonian is

$$\mathscr{H}^R=\omega_Q[I_z^2-\tfrac{1}{3}I(I+1)]-\omega_R[I_z\cos(\theta)+I_x\sin(\theta)]. \tag{8}$$

As before, this Hamiltonian can be greatly simplified if we assume that the rotation is adiabatic, and this approximate adiabatic Hamiltonian has eigenvalues of

$$\omega_Q\pm\tfrac{3}{2}\omega_R\cos(\theta),\quad -\omega_Q\pm\tfrac{1}{2}\omega_R\zeta, \tag{9}$$

where

$$\zeta=\sqrt{\cos^2(\theta)+4\sin^2(\theta)}=\sqrt{4-3\cos^2(\theta)}. \tag{10}$$

(The significance of this form for ζ is discussed further in the section on magnetic fields below.) In this case the signal intensities also depend on θ, and the calculated NQR signal is

$$s(t)=2+3\cos^2(\theta)+3\sin^2(\theta)\cos(2\omega_Q t)f(t), \tag{11}$$

where

$$f(t)=\frac{\zeta+\cos(\theta)}{2\zeta}\cos\left[\omega_R t\left(\frac{3\cos(\theta)-\zeta}{2}\right)\right]+\frac{\zeta-\cos(\theta)}{2\zeta}\cos\left[\omega_R t\left(\frac{3\cos(\theta)+\zeta}{2}\right)\right]. \tag{12}$$

The NQR line is, in general, split into four components, as shown in Fig. 2. However, there are several special cases in which the number of lines is reduced. First, consider rotation around the quadrupolar axis, $\theta=0$. In this case the quadrupolar lines are split into two. However, using the excitation and detection scheme described above, the quadrupolar lines will have zero intensity, and so this limit is not very interesting. Second, for rotation at the magic angle ($\theta=\arccos(\sqrt{1/3})$) Eq. (12) simplifies to

$$f(t)=\tfrac{2}{3}+\tfrac{1}{3}\cos(\sqrt{3}\omega_R t), \tag{13}$$

corresponding to a triplet with intensities 1:4:1. This situation is equivalent to that studied by Tycko[6] using single crystal ^{35}Cl NQR studies of sodium chlorate. Finally, consider rotation around an axis perpendicular to the quadrupolar axis, that is, $\theta=\pi/2$. This is just the simple case described by Eq. (3), and Eq. (12) simplifies to $f(t)=\cos(\omega_R t)$ as expected, giving rise to a two line spectrum.

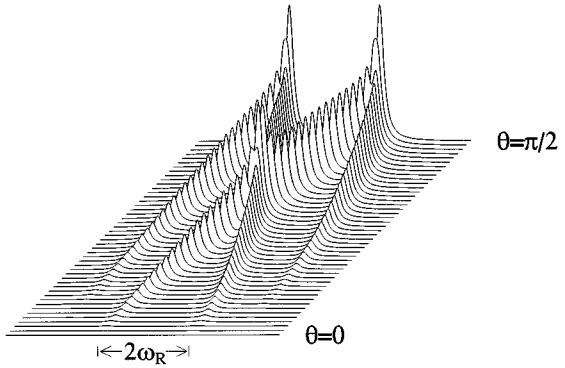

FIG. 2. Calculated spectra from xenon atoms in a cylindrical container undergoing rotation around an axis at an angle θ to the cylinder axis; an expansion around one of the quadrupolar transitions is shown. Note that this figure includes the effects of the $\sin^2(\theta)$ intensity weighting predicted for the excitation and detection scheme described. In general, the quadrupolar line is split into four, but as $\theta\to 0$, the intensity of the two outer lines tends to zero, while as $\theta\to 90°$ the inner and outer lines overlap. The splitting between the inner pair of lines changes sign as θ is increased, and at the magic angle this splitting passes through zero, resulting in a three line spectrum.

III. INCOHERENT MOTION

As described above, coherent motion of the quadrupole axis can give rise to line splittings. Now suppose that the motion is incoherent, and different for each nucleus in the sample. In this case each nucleus will experience different and varying splittings, giving rise to inhomogeneous line broadening.

This situation cannot arise in the system described above: As the motion of the quadrupole axis is due to the macroscopic motion of the sample container, each nucleus will experience the same motion. It can, however, arise in a related system involving the diffusion of ^{131}Xe gas around a toroidal container.

The local geometry of a torus is like that of a cylinder, and so a ^{131}Xe nucleus at some point in the torus will experience an average quadrupolar coupling with near cylindrical symmetry (Fig. 3). The symmetry axis lies along the apparent cylinder axis, that is, tangential to the torus. As the xenon atom moves round the torus, the direction of its quadrupole axis will vary, and this variation takes the form of rotation around an axis threading the torus, perpendicular to the quadrupole axis. This situation is identical to that described above, and so each nucleus will acquire Berry phases, but as

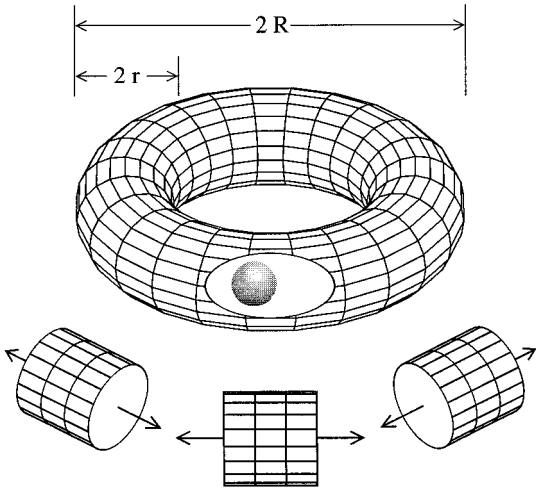

FIG. 3. Schematic depiction of a xenon atom in a torus. As long as the tube radius, r, is small compared with the torus radius, R, the xenon nucleus experiences an average electric field gradient with local cylindrical symmetry. Hence the nucleus has an axially symmetric quadrupolar coupling to the container, with a symmetry axis directed along the local cylinder axis, that is tangential to the torus. As the atom moves around the torus the local cylinder axis changes, causing the quadrupole axis to rotate.

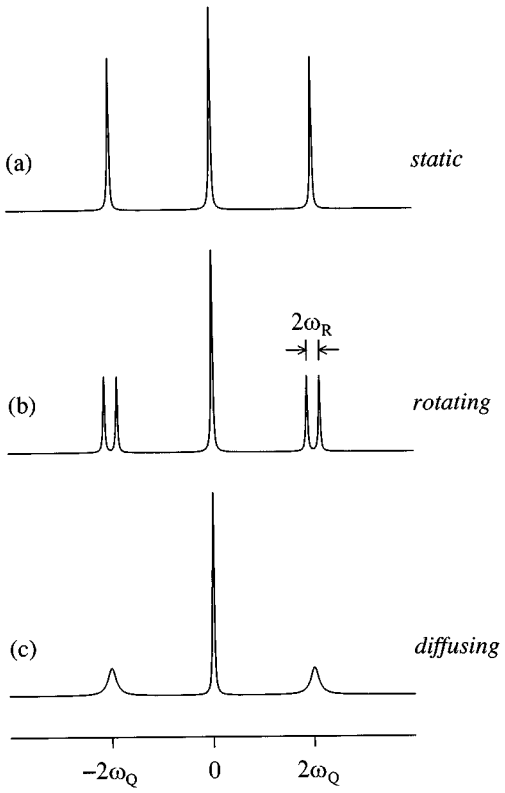

FIG. 4. Calculated spectra for ^{131}Xe nuclei in a toroidal container. Static nuclei only experience the quadrupolar interaction, and so give a simple three line spectrum (a). Nuclei which move around the torus at a constant rate experience a fictitious magnetic field which splits the quadrupolar transitions (b). Diffusive motion of nuclei around the torus corresponds to an incoherent distribution of rotation rates, and so gives line broadenings (c) instead of splittings.

the phases acquired are different for different nuclei the effect will appear as line broadening instead of splittings (Fig. 4).

During any short period of time, the motion of any given xenon atom can be considered constant, and so the effect on the nuclear Hamiltonian is that of steady rotation at a frequency ω_R. Over an extended period this frequency will vary. However, the total phase acquired by an eigenstate during any time period depends only on the average rotation rate, $\overline{\omega_R}$, during that time, even for the non-Abelian case of degenerate states.[17,18] Hence for any given nucleus

$$s(t)=2+3\cos(2\omega_Q t)\cos(\overline{\omega_R}t). \tag{14}$$

This can be simplified by writing $w=\overline{\omega_R}t$, giving

$$s(t)=2+3\cos(2\omega_Q t)\cos(w), \tag{15}$$

where w, called the winding, is the total angular distance traveled by a nucleus. This simple form can be easily rationalized. For a geometric phase shift, such as a Berry phase, the phase shift depends only on the path traveled, and is independent of the way in which the system moves along that path. The $\cos(w)$ dependence arises from interference between signals from the two different quadrupolar transitions, which acquire equal and opposite phase shifts of $\pm w$.

The winding, w, is related to the conventional winding number, n, by $w=2\pi n+\phi$, where ϕ is any additional fractional rotation. The periodicity of the cosine function in Eq. (15) shows that the behavior of the system is independent of the winding number achieved by an individual nucleus, but depends only on the additional fractional rotation. This suggests two possible types of experiment which might allow these Berry phases to be detected.

The first class of experiment involves selective excitation and detection of specific nuclei. Suppose we excite all the nuclei in a small region of the torus, and then detect signals from nuclei in a different region, at an angular distance ϕ around the torus. Clearly, signals will only be detected from nuclei which have diffused from the excitation region to the detection region, and so the signal intensity will depend on the extent of such diffusion. However, any nuclei which are detectable must have acquired Berry phases corresponding to motion through an angle ϕ, and so the signal intensity will also be modulated by a $\cos(\phi)$ term. In particular, it should not be possible to detect any signal from nuclei which have traveled a quarter of the way round the torus, where $\cos(\pi/2)=0$.

The second class of experiments involves excitation and detection of all the nuclei in the torus. In this case nuclei with different windings will be detected, and the total signal will depend on the probability distribution of acquired windings. The motion of gas atoms around a torus can be described by one dimensional diffusion, with a probability density function[19]

$$\mathscr{P}(w)=\frac{1}{2\sqrt{\pi\ dt}}\exp(-w^2/4\ dt), \tag{16}$$

where d is the one-dimensional diffusion coefficient mea-

sured in rad^2 s^{-1}. Multiplying Eqs. (15) and (16) together and integrating over all possible windings gives the total observable signal

$$S(t)=\int \mathscr{P}(w)s(t)dw \tag{17}$$

$$=2+3\cos(2\omega_Q t)\exp(-dt), \tag{18}$$

showing that the signal from the quadrupolar transitions decays exponentially with a rate equal to the diffusion coefficient (the central line, which is not split by the fictitious field, remains unbroadened). Note that this decay occurs not because nuclei acquire large winding numbers, but because the distribution of fractional windings becomes asymptotically flat.

The one-dimensional diffusion coefficient, d, is related to the conventional three-dimensional diffusion constant, D, by $d=D/3R^2$, where R is the radius of the torus (see Fig. 3). For xenon at standard temperature and pressure[20] $D\approx 5\times 10^{-6}$ m^2 s^{-1}, so a torus with a radius of a few millimetres will have a Berry dephasing time constant of a few seconds, shorter than that of other relaxation mechanisms. In such a torus the typical rotation rate will be smaller than the quadrupolar coupling, and so the adiabatic approximation is reasonable. Small deviations from adiabaticity will result in a slightly faster loss of signal, but at very high diffusion rates the signal should once again become sharp, as predicted by average Hamiltonian theory.[21]

An interesting analogy exists between our system and one discussed recently by Goldman, Fleury, and Guéron.[22] They consider the effect of rotating a sample around an axis parallel to the static field while observing its conventional high field NMR spectrum. When a conventional radio frequency coil is used for excitation and detection, such rotation has no effect (assuming that the static field is homogeneous). If, however, the radio frequency coil produces a field radial to the static field, sample rotation results in a shift in the NMR frequency equal to the rotation rate. This is exactly the result expected for a fictitious field along the rotation axis. They predict that similar effects would be seen for motion of a toroidal sample within a solenoidal radio frequency coil wrapped around the torus. Finally, they consider the effect of incoherent motion, such as diffusion of the sample within a toroidal container. In this case they predict that the random distribution of phase shifts should result in signal loss.

The signal from a toroidal sample rotating at a constant frequency, ω_R, is

$$s(t)=\exp(i\omega_0 t)\exp(-i\omega_R t), \tag{19}$$

where ω_0 is the Larmor frequency and the initial amplitude and the effects of relaxation have been ignored. As before, for incoherent motion the total phase acquired depends only on the average rotation rate, $\overline{\omega_R}$, and hence the winding, $w=\overline{\omega_R}t$. For an ensemble of molecules each undergoing random diffusion we can apply Eqs. (17) and (16) to obtain

$$S(t)=\exp(i\omega_0 t)\exp(-dt), \tag{20}$$

making clear the analogy with Eq. (18).

IV. COHERENCE DEPHASING

The discussion in the previous section shows that incoherent motion can lead to the random acquisition of Berry phases, and thus to a loss of signal coherence. Recently, Serebrennikov and Steiner have described a more general approach,[23–25] which can be applied to many types of incoherent motion, including the diffusive motion of gas in a torus.

Serebrennikov and Steiner start from the gauge field, which in zero-field magnetic resonance takes the form of a fictitious magnetic field. If the gauge field commutes with the main Hamiltonian, then evolution under the two terms can be considered separately. They then use the Fano–Zwanzig projection operator method[23,26,27] to calculate an ensemble averaged propagator for evolution under the incoherent gauge field,

$$\frac{d}{dt}\langle\rho(t)\rangle=\int_0^t\langle\hat{A}(t)\hat{A}(t')\rangle\langle\rho(t')\rangle dt', \tag{21}$$

where $\hat{A}(t)$ is the super operator corresponding to the gauge field, and for continuous rotation $\hat{A}=-i\omega_R\hat{I}_\alpha$. If the correlation time of the motion is short compared to the rate of change of $\rho(t)$, Eq. (21) can be approximated by

$$\frac{d}{dt}\langle\rho(t)\rangle=\int_0^t\langle\hat{A}(t)\hat{A}(t')\rangle dt'\langle\rho(t)\rangle, \tag{22}$$

and the problem reduces to calculating the integral

$$\int_0^t\langle\hat{A}(t)\hat{A}(t')\rangle dt'. \tag{23}$$

Clearly, the value of this integral depends on the form of the motion. For motion around a torus $\hat{A}=-i\omega_R\hat{I}_x$, and at any point in time the angular velocities of the individual atoms will have a Maxwell distribution. Now suppose that at intervals τ the motion of each atom changes such that the velocities still have a Maxwell distribution but the velocities before and after the change are completely uncorrelated. In this case

$$\int_0^t\langle\hat{A}(t)\hat{A}(t')\rangle dt'=-\frac{c^2\tau}{2}\hat{I}_x^2, \tag{24}$$

where c is the root mean square velocity (in rad s^{-1}).

In general, the gauge field does not commute with the main Hamiltonian. However, as long as the motion is slow I_x may be replaced by its ''adiabatic'' form

$$I_x'=\begin{pmatrix}0&0&0&0\\0&0&1&0\\0&1&0&0\\0&0&0&0\end{pmatrix}. \tag{25}$$

This *does* commute with the quadrupolar Hamiltonian, and so the method can be used. The eigenvalues of $-\hat{I}_x'^2$ are real and negative, and so this operator should cause coherence dephasing. This is confirmed by detailed calculation: Combining evolution under the two operators gives

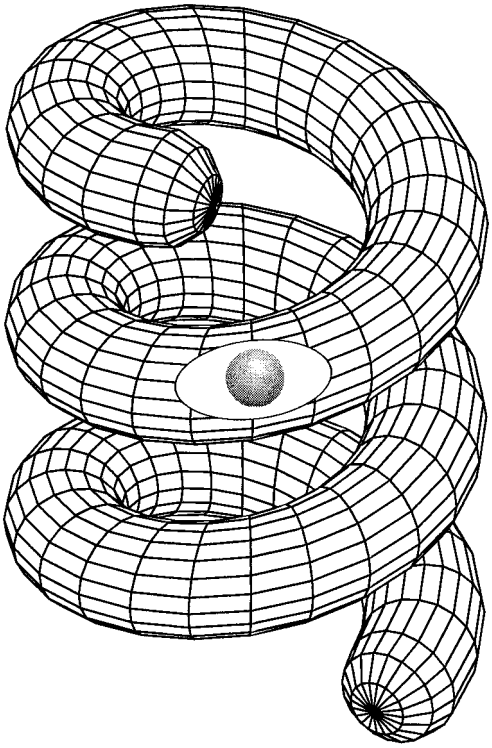

FIG. 5. Schematic depiction of a xenon atom in a helical container. A xenon nucleus far from the ends of the helix experiences a average electric field gradient with local cylindrical symmetry, and so has an axially symmetric quadrupolar coupling with a symmetry axis directed tangential to the helix.

$$\rho(t)=\exp[i\omega_Q(\hat{I}_z^2-\tfrac{1}{3}I(I+1))t-(c^2\tau\hat{I}_x'^2/2)t]\rho(0), \tag{26}$$

and starting from and detecting I_x gives

$$s(t)=2+3\cos(2\omega_Q t)\exp(-(c^2\tau/2)t), \tag{27}$$

which has the same form as Eq. (18).

In fact, the two Eqs. (18) and (27) are completely equivalent, as shown below. For diffusive motion, described by Eq. (16), the root mean square distance moved by any particular atom during a time τ is $\sqrt{2\,d\,\tau}$. During this time the atom has an ''apparent velocity'' equal to the distance it has moved divided by τ. Clearly, this apparent velocity has a Maxwell distribution, with a root mean square apparent velocity of

$$c=\frac{\sqrt{2\,d\,\tau}}{\tau}=\sqrt{\frac{2d}{\tau}}. \tag{28}$$

Equation (27) then predicts a dephasing rate of

$$\frac{c^2\tau}{2}=\frac{2d}{\tau}\times\frac{\tau}{2}=d, \tag{29}$$

identical to that in Eq. (18).

V. MOTION IN A HELIX

Similar, but more complex behavior should emerge if the xenon gas is placed in a cylindrical container which has been wound into a helix (Fig. 5). Nuclei in the helix will experience an average quadrupolar coupling which is cylindrically symmetric, with the symmetry axis tangential to the helix. Motion of gas molecules around the helix will cause the quadrupolar axis to rotate, but the axis about which this rotation occurs is not perpendicular to the quadrupole axis, as was the case for the torus. Instead the rotation axis, and hence the axis of the fictitious field, is directed at some angle, θ, to the quadrupole axis, where θ depends on the pitch of the helix.

Clearly, this situation is equivalent to the case of the rotating cylinder, described in Eq. (8), and so the signal will be described by Eqs. (11) and (12). As before, we can replace the rotation rate by its average value, and then write $w=\overline{\omega_R}t$. Hence

$$f(t)=\frac{\zeta+\cos(\theta)}{2\zeta}\cos\left[w\left(\frac{3\cos(\theta)-\zeta}{2}\right)\right]+\frac{\zeta-\cos(\theta)}{2\zeta}\cos\left[w\left(\frac{3\cos(\theta)+\zeta}{2}\right)\right]. \tag{30}$$

Unlike a torus, a helical container has ends, and so the motion of gas atoms is described by bounded diffusion, rather than free diffusion. In the limit of infinite length, however, this becomes irrelevant, and Eq. (16) remains applicable. Hence

$$S(t)=2+3\cos^2(\theta)+3\sin^2(\theta)\cos(2\omega_Q t)F \tag{31}$$

with

$$F=\frac{\zeta+\cos(\theta)}{2\zeta}\exp\left[-dt\left(\frac{3\cos(\theta)-\zeta}{2}\right)^2\right]+\frac{\zeta-\cos(\theta)}{2\zeta}\exp\left[-dt\left(\frac{3\cos(\theta)+\zeta}{2}\right)^2\right]. \tag{32}$$

In general, the decay of signal intensity is biexponential. As expected, Eq. (32) simplifies to $F=\exp(-dt)$ for the case of a torus ($\theta=\pi/2$) and

$$F=\tfrac{2}{3}+\tfrac{1}{3}\exp(-3dt) \tag{33}$$

for a helix at the magic angle.

As with the case of the torus, it should be possible to perform experiments to detect geometric dephasing in helices. Indeed, the behavior of ^{131}Xe in helical containers should provide an excellent test, as the predicted biexponential relaxation should provide an unambiguous indicator of these effects. The case of a helix close to the magic angle is particularly sensitive, as the two dephasing time constants are expected to be very different.

These calculations can also be performed using the coherence dephasing formalism of Serebrennikov and Steiner.[23–25] In this case

$$\hat{A}=-i\omega_R(\hat{I}_z\cos(\theta)+\hat{I}_x\sin(\theta)). \tag{34}$$

Making the same assumptions as before (Sec. IV) gives

$$F=\frac{\zeta+\cos(\theta)}{2\zeta}\exp\left[-\frac{c^2\tau}{2}t\left(\frac{3\cos(\theta)-\zeta}{2}\right)^2\right]+\frac{\zeta-\cos(\theta)}{2\zeta}\exp\left[-\frac{c^2\tau}{2}t\left(\frac{3\cos(\theta)+\zeta}{2}\right)^2\right], \quad (35)$$

which is clearly equivalent to Eq. (32) with $d=c^2\tau/2$.

The equations above have all been written using variables which are convenient for the calculations involved, but which may not be convenient for describing actual helical containers. Any helical container may be formed from a tube of length L wrapped in a helix around a cylinder of radius R (assumed to be much greater than the tube radius, r). Suppose the fractional pitch of the helix is p (so that the height of the helix is $p\times L$). Then the helix angle is

$$\theta=\arccos\left(\frac{p}{\sqrt{1+p^2}}\right), \quad (36)$$

the angular length of the helix is

$$\psi=\frac{L}{R\sqrt{1+p^2}}, \quad (37)$$

and the angular diffusion constant is

$$d=\frac{D}{3R^2(1+p^2)}, \quad (38)$$

where D is the conventional three-dimensional diffusion constant. Note that in the limit $p\to 0$ these reduce to $\theta=\pi/2$, $\psi=L/R$, and $d=D/3R^2$ as expected for a torus.

VI. MOTION IN SHORT HELICES AND TRUNCATED TORUSES

The discussion above concerning the motion of nuclei in helical containers depends on the assumption that the container is infinitely long, so that end effects can be ignored. While this greatly simplifies calculations, and is probably appropriate for helical containers with many turns, it clearly cannot be applied to the motion of nuclei in short containers.

This problem is most conveniently approached using the concept of winding, developed in Sec. III. For finite helices

$$S(t)=\int \mathscr{P}(w,\psi)s(t)dw, \quad (39)$$

where the probability density function for windings now depends on the angular length of the helix [ψ, see Eq. (37)], and $s(t)$ is given by Eqs. (11) and (12) as before. The expression for $\mathscr{P}(w,\psi)$ is complicated as the equations for hindered diffusion must be used, but the problem can be easily solved numerically. The results for two specific cases are shown in Fig. 6. These cases involve truncated toruses (that is, $\theta=\pi/2$), but similar results occur for other types of short helix. This nonexponential relaxation may provide another possible experimental test of our predictions.

A simple analytical solution *can* be obtained for the limiting signal from a short helix at infinite time. Individual nuclei may start anywhere in the helix, with a flat distribution of initial positions, and at very long times the distribution of final positions will be flat and independent of the starting position. The distribution of acquired windings, however, will not be flat, as the range of windings which may be achieved depends on the starting position of each nucleus. Integrating over all possible initial positions gives

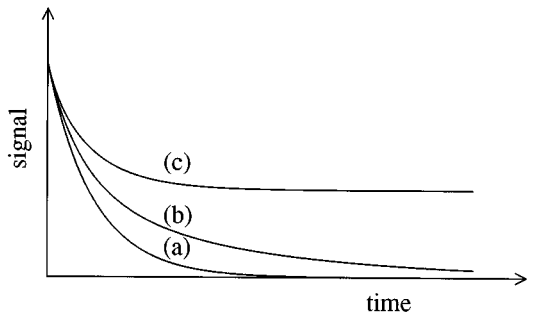

FIG. 6. Geometric dephasing due to diffusion of xenon atoms around a torus causes the quadrupolar signal to decay exponentially to zero (a). The signal from a tube bent around a torus, but without the ends joined ($\psi=2\pi$), decays more slowly but eventually reaches zero (b). If the tube is bent round a half torus ($\psi=\pi$) the signal decays to a constant value (c).

$$\lim_{t\to\infty}\mathscr{P}(w,\psi)=\frac{1}{\psi}\left(1-\frac{|w|}{\psi}\right) \quad (40)$$

(note that for a true torus $\psi=\infty$, as the motion is unbounded). Hence

$$F=\frac{1}{4\psi^2(3\cos^2(\theta)-1)^2}\left[8(3\cos^2(\theta)+1)-\left(\frac{(\cos(\theta)+\zeta)(3\cos(\theta)+\zeta)^2}{\zeta}\right)\cos\left(\frac{\psi(3\cos(\theta)-\zeta)}{2}\right)+\left(\frac{(\cos(\theta)-\zeta)(3\cos(\theta)-\zeta)^2}{\zeta}\right)\cos\left(\frac{\psi(3\cos(\theta)+\zeta)}{2}\right)\right]. \quad (41)$$

As usual, this equation can be greatly simplified at particular values of θ. For a helix of zero pitch ($\theta=\pi/2$),

$$F=\mathrm{sinc}^2(\psi/2), \quad (42)$$

where $\mathrm{sinc}(x)=\sin(x)/x$. The limiting signal is zero when $\psi=2\pi$, as seen in Fig. 6. Similarly, for a helix at the magic angle

$$F=\tfrac{2}{3}+\tfrac{1}{3}\,\mathrm{sinc}^2(\sqrt{3}\psi/2). \quad (43)$$

VII. THE EFFECT OF MAGNETIC FIELDS

Finally, we consider the effects of additional applied magnetic fields. While such fields could be applied along any axis, an interesting case involves fields directed parallel or perpendicular to the quadrupolar axis. For simplicity we consider only systems in which the rotation axis is perpendicular to the quadrupolar axis; in the absence of additional magnetic fields, such systems are described by equations of the

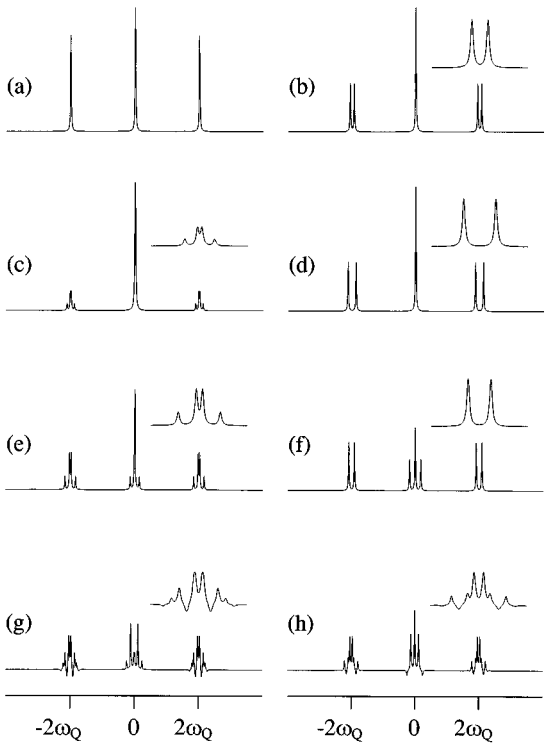

FIG. 7. Calculated spectra from ^{131}Xe nuclei in a cylindrical container undergoing coherent rotation in the presence of a magnetic field. For all spectra except (a) the right-hand multiplet is also shown on an expanded horizontal scale. (a) No rotation and no magnetic field; the quadrupolar transitions at $\pm 2\omega_Q$ are unsplit. (b) The effect of rotation around an axis perpendicular to the quadrupolar axis; the quadrupolar lines are split into two by the fictitious field [Eq. (7)]. (c) The effect of rotation around an axis at an angle of 45° to the quadrupolar axis; the quadrupolar lines are split into four and the line intensities are affected [Eqs. (11) and (12)]. Note that the central line has been truncated. (d) As case (b), but with an additional static magnetic field applied parallel to the fictitious field; the two fields sum together increasing the splitting of the quadrupolar lines [Eq. (44)]. (e) As case (b), but with an additional static magnetic field applied parallel to the quadrupolar axis; this results in an apparent tilt of the rotation axis, and a spectrum similar to that seen in (c). (f) As case (b), but with an additional static magnetic field applied perpendicular to the quadrupolar and rotation axes; this augments the fictitious field, but also results in the central line being split. (g) and (h) As case (b), but with an additional static magnetic field applied perpendicular to the rotation axis and with a static orientation in the laboratory frame. In the rotating frame this field appears to rotate in the yz plane, modulating the Hamiltonian and creating modulation sidebands in the spectrum. The detailed form of the spectrum depends on the initial orientation of the applied field with respect to the quadrupolar axis; (g) corresponds to a perpendicular initial orientation, while (h) corresponds to a parallel initial orientation.

form of Eq. (3). In the case of incoherent motion this corresponds to xenon atoms in toroidal containers. The results for coherent motion are depicted in Fig. 7.

The simplest case is when the field is applied parallel to the rotation axis (perpendicular to the quadrupolar axis and parallel to the fictitious field). In this case the applied and fictitious fields simply sum together, and so for coherent motion of nuclei around the torus

$$s(t)=2+3\cos(2\omega_Q t)\cos(\omega_R t+\omega_M t), \tag{44}$$

where ω_M is the strength of the applied magnetic field [see Fig. 7(d)]. As before, incoherent motion is treated by writing $w=\overline{\omega_R}t$ and integrating over $\mathscr{P}(w)$, giving

$$S(t)=2+3\cos(2\omega_Q t)\cos(\omega_M t)\exp(-dt). \tag{45}$$

The effects of the fictitious and applied magnetic fields have the same form, and so can be treated separately. The fictitious field creates line broadening as before, while the applied magnetic field splits the (broadened) quadrupolar lines into a doublet.

Alternatively, since the applied and fictitious fields have the same form, the applied magnetic field can be treated as a fictitious motion around the torus. Unlike the real physical motions of the different nuclei, this fictitious motion is *identical* for all the nuclei in the torus, and so must produce splittings rather than broadenings. For this reason magnetic fields cannot be used to remove the effects of incoherently acquired Berry phases (they *can* be used to remove the effects of coherently acquired Berry phases, as demonstrated by Tycko[6]).

Another simple case is when the applied field is directed parallel to the quadrupolar axis (this could be achieved by wrapping a solenoidal coil around the container). The signal can be calculated directly as

$$\begin{aligned} s(t)=&\frac{2\omega_R^2}{\omega_F^2}+\frac{\omega_M^2}{2\omega_F^2}\cos(\omega_F t)+3\cos(2\omega_Q t)\\ &\times\left[\cos\left(\frac{3\omega_M t}{2}\right)\cos(\omega_F t)\right.\\ &\left.+\frac{\omega_M}{2\omega_F}\sin\left(\frac{3\omega_M t}{2}\right)\sin(\omega_F t)\right], \end{aligned} \tag{46}$$

where

$$\omega_F=\sqrt{(\omega_M/2)^2+\omega_R^2}=\tfrac{1}{2}\sqrt{\omega_M^2+(2\omega_R)^2} \tag{47}$$

is the total effective field strength. Note that, as expected, Eq. (46) reduces to Eq. (7) when $\omega_M\rightarrow 0$.

The form of Eq. (47) might seem unusual: Why should the applied field be divided by two, while the fictitious field is not? In fact, this effect has already been discussed in Sec. II above. The fictitious magnetic field (perpendicular to the quadrupolar axis) is selective for the central transition, and so its effective field strength is increased by a factor of 2. The applied magnetic field (parallel to the quadrupolar axis) affects all the transitions, and so its field strength is not doubled in this way.

Another approach to this problem is to notice that just as a magnetic field applied along the rotation axis is equivalent to a fictitious motion, a magnetic field along the quadrupolar axis is equivalent to a fictitious tilt of the rotation axis, or the conversion of the torus into a helix. This fictitious tilt can be described by an apparent field strength, ω_B, and an apparent tilt angle, θ, where

$$\omega_R=\omega_B\sin(\theta) \tag{48}$$

and

$$\omega_M = \omega_B \cos(\theta) \tag{49}$$

as before. Inserting these forms into Eq. (47) gives

$$\omega_F = \tfrac{1}{2}\omega_B \sqrt{\cos^2(\theta) + 4\sin^2(\theta)} = \tfrac{1}{2}\omega_B \zeta, \tag{50}$$

where ζ is defined as before [see Eq. (10)]. This origin of this form for ζ is now clear.

Substituting the above into Eq. (46) gives, after extensive rearrangement,

$$s(t) = \frac{8\sin^2(\theta)}{\zeta^2} + \frac{2\cos^2(\theta)}{\zeta^2}\cos\left(\frac{\omega_B t \zeta}{2}\right) + 3\cos(2\omega_Q t) f(t) \tag{51}$$

with

$$f(t) = \frac{\zeta + \cos(\theta)}{2\zeta}\cos\left[\omega_B t\left(\frac{3\cos(\theta) - \zeta}{2}\right)\right] + \frac{\zeta - \cos(\theta)}{2\zeta}\cos\left[\omega_B t\left(\frac{3\cos(\theta) + \zeta}{2}\right)\right]. \tag{52}$$

The similarity to Eqs. (11) and (12) is obvious. The results are not identical because the excitation and detection schemes are not the same: For the true tilted system the initial state and detection operator were assumed to lie along the tilted rotation axis (at some angle to the quadrupolar axis), while in this fictitious system the initial state and detection operator lie along the untilted rotation axis (which is perpendicular to the quadrupolar axis). This changes the line intensities, and also produces the splitting of the line at zero-frequency [Fig. 7(c)].

As before, the fictitious helix also differs from a real helix in that the applied magnetic field is the same for all nuclei. Since the apparent tilt angle depends on the relative sizes of ω_R and ω_M, this angle will be different for different nuclei in the sample; indeed it will be different for the same nucleus at different times. For this reason it is difficult to calculate the effects of incoherent motion, as the simple approaches used above are no longer applicable. It should be possible to use the approach of Serebrennikov and Steiner, with an explicit evaluation of Eq. (23).

Third, we consider the effects of a magnetic field applied perpendicular to the quadrupolar and rotation axes (the y axis in our usual notation). For a toroidal container this corresponds to a field in the plane of the torus, and everywhere perpendicular to it. For a field along the y axis the resulting signal is

$$s(t) = \frac{2\omega_R^2 + 2\omega_M^2\cos(2\omega_F t)}{\omega_F^2} + 3\cos(2\omega_Q t)\cos(\omega_F t), \tag{53}$$

where ω_M is the applied field strength as before, but in this case

$$\omega_F = \sqrt{\omega_R^2 + \omega_M^2}, \tag{54}$$

in contrast to the form given in Eq. (47). In the present case *both* the applied and fictitious fields are selective for the central transition, and so both field strengths are doubled.

The effect of an applied field along the y axis is similar to that of a field along the rotation axis (the x axis), in that the applied field augments the fictitious field. Since, however, the applied and fictitious fields are now perpendicular it is necessary to use a vector sum to calculate the effective field strength. Furthermore, the initial state and detection operator are no longer parallel to the effective field axis, and so the signal is subtly changed [see Fig. 7(f)]. In particular, the central (zero-frequency) transition is split into three components, as in the case of the fictitious helix arising from fields directed parallel to the quadrupolar axis. Once again the fixed magnitude of the applied field results in varying effective fields, and so makes it difficult to calculate the effects of incoherent motion.

Finally, we consider the effects of a field perpendicular to the rotation axis, but with a fixed direction in the laboratory frame. In our transformed coordinate system, the direction of this field will vary as the container is rotated or as nuclei move around the torus: The field can be parallel to the quadrupolar axis (along z), perpendicular to it (along y), or along some other direction in the yz plane. The Hamiltonian varies constantly, even for rotation at a constant rate, and the Hamiltonian no longer commutes with itself at different times; thus the simple approach embodied in equation 6 is not possible, and it is necessary to perform an explicit time-ordered integration. The instantaneous effect of the applied field will be some combination of a fictitious additional motion and a fictitious tilt, as described above, but rotation of the container will results in modulation of the Hamiltonian, and so modulation sidebands at multiples of the rotation rate are expected in addition to any splittings arising from the real and fictitious fields.

For this system the calculated spectrum depends not only on the rotation rate and the strength of the applied field, but also on the initial orientation of the quadrupolar axis with respect to this field. Spectra are shown in Fig. 7 for two different orientations: (g) shows the spectrum when the applied field initially lies along the y axis, while (h) shows the spectrum when the applied field initially lies along the z axis. While both spectra show similar modulation side bands, they differ in many fine details. For the case of motion around a torus it would be necessary to average the signal over all initial orientations. This system is related to the behavior of spin-$\frac{3}{2}$ holes in GaAs.[28]

VIII. SUMMARY

Zero-field magnetic resonance experiments differ from those in high field in that the absence of an external field renders many interactions isotropic. In this situation, although the eigenvalues of the spin Hamiltonian are unaffected by slow motion of the system such motion *can* result in the acquisition of Berry phase shifts and the mixing of degenerate states. While coherent motion typically results in frequency shifts and splittings, incoherent motion will generally result in coherence dephasing, and hence spin relaxation and line broadening. We have calculated the nature and

extent of this broadening in a variety of simple model systems, and discussed possible experiments for detecting these effects.

The loss of signal coherence as a result of the random acquisition of geometric phases may also be important in other NQR experiments, as well as in high field NMR.[22] In particular, Berry phases arising from the slow rotational diffusion of particles could be an important source of relaxation in conventional NQR studies of colloids.[29]

ACKNOWLEDGMENTS

We would like to thank Y. Lyanda-Geller, D. P. Arovas, S. Appelt, and M. Mehring for many stimulating discussions. We also grateful to M. Ernst for much helpful advice. J. A. Jones would like to thank C. M. Dobson for his encouragement and support. This work was supported by the Director of the Office of Energy Research, Office of Basic Energy Sciences, Materials Sciences Division of the U.S. Department of Energy, under Contract No. DE-AC03-76SF00098.

[1] M. V. Berry, Proc. R. Soc. London, Ser. A **392**, 45 (1984).
[2] *Geometric Phases in Physics*, edited by A. Shapere and F. Wilczek (World Scientific, Singapore, 1989).
[3] J. W. Zwanziger, M. Koenig, and A. Pines, Annu. Rev. Phys. Chem. **41**, 601 (1990).
[4] T. Bitter and D. Dubbers, Phys. Rev. Lett. **59**, 251 (1987).
[5] D. Suter, K. T. Mueller, and A. Pines, Phys. Rev. Lett. **60**, 1218 (1988).
[6] R. Tycko, Phys. Rev. Lett. **58**, 2281 (1987).
[7] P. Härle, G. Wäckerle, and M. Mehring, Appl. Magn. Reson. **5**, 207 (1993).
[8] J. A. Jones and A. Pines, Chem. Phys. Lett. **247**, 215 (1995).
[9] For example, L. J. Schiff, *Quantum Mechanics*, 3rd ed. (McGraw-Hill, Singapore, 1968).
[10] Z. Wu, W. Happer, and J. M. Daniels, Phys. Rev. Lett. **59**, 1480 (1987).
[11] D. Raftery, H. W. Long, D. Shykind, P. J. Grandinetti, and A. Pines, Phys. Rev. A **50**, 567 (1994).
[12] S. Appelt, G. Wäckerle, and M. Mehring, Phys. Rev. Lett. **72**, 3921 (1994).
[13] S. Appelt, G. Wäckerle, and M. Mehring, Phys. Lett. A **204**, 210 (1995).
[14] A. Abragam, *Principles of Nuclear Magnetism* (Clarendon, Oxford, 1961).
[15] S. Vega, J. Chem. Phys. **68**, 5518 (1978).
[16] A. Wokaun and R. R. Ernst, J. Chem. Phys. **67**, 1752 (1977).
[17] A. Zee, Phys. Rev. A **38**, 1 (1988).
[18] J. W. Zwanziger, M. Koenig, and A. Pines, Phys. Rev. A **42**, 3107 (1990).
[19] Not as we erroneously stated in Ref. 8.
[20] P. W. E. Peereboom, H. Luigjes, and K. O. Prins, Physica A **156**, 260 (1989).
[21] P. Meier, G. Kothe, P. Jonsen, M. Trecoske, and A. Pines, J. Chem. Phys. **87**, 6867 (1987).
[22] M. Goldman, V. Fleury, and M. Guéron, J. Magn. Reson. A **118**, 11 (1996).
[23] Yu. A. Serebrennikov and U. E. Steiner, Chem. Phys. Lett. **222**, 309 (1994).
[24] U. E. Steiner and Yu. A. Serebrennikov, J. Chem. Phys. **100**, 7503 (1994).
[25] Yu. A. Serebrennikov and U. E. Steiner, J. Chem. Phys. **100**, 7508 (1994).
[26] U. Fano, Phys. Rev. **131**, 259 (1963).
[27] R. Zwanzig, Physica **30**, 1109 (1964).
[28] Y. Lyanda-Geller and D. P. Arovas (private communication).
[29] J. Jeener, J. D. Bell, P. Broekaert, E. Dumont, and M. Koenig, Adv. Magn. Reson. **14**, 95 (1990).